# Passive runaway electron suppression in tokamak disruptions

H. M. Smith,[1,*] A. H. Boozer,[2,3] and P. Helander[1]

[1] *Max-Planck/Princeton Center for Plasma Physics,*
*Max-Planck-Institut für Plasmaphysik, 17491 Greifswald, Germany*

[2] *Max-Planck/Princeton Center for Plasma Physics,*
*Princeton Plasma Physics Laboratory,*
*Princeton, New Jersey 08540, USA*

[3] *Department of Applied Physics and Applied Mathematics,*
*Columbia University, New York, New York 10027, USA*

## Abstract

Runaway electrons created in disruptions pose a serious problem for tokamaks with large current. It would be desirable to have a runaway electron suppression method which is passive, i.e. a method that does not rely on an uncertain disruption prediction system. One option is to let the large electric field inherent in the disruption drive helical currents in the wall. This would create ergodic regions in the plasma and increase the runaway losses. Whether these regions appear at a suitable time and place to affect the formation of the runaway beam depends on disruption parameters, such as electron temperature and density. We find that it is difficult to ergodize the central plasma before a beam of runaway current has formed. However, the ergodic outer region will make the Ohmic current profile contract, which can lead to instabilities that yield large runaway electron losses.

*Electronic address: hakan.smith@ipp.mpg.de

## I. INTRODUCTION

The greater the plasma current is before a disruption, the more efficiently the avalanche runaway mechanism can convert it into a beam of runaway electron current [1–3]. Runaway electrons therefore pose a serious threat to the operation of future tokamaks with large current, such as ITER. The kinetic energy of the runaways is sufficiently high (tens of MeV) that the runaway beam can cause severe damage if it impacts on the vessel due to loss of position control. Moreover, as the runaway electron beam drifts toward the wall and is "scraped off" against it, a substantial part of the energy contained in the poloidal magnetic field can be transferred to the runaway electrons, thus further increasing their capacity for damage [4]. It is therefore essential to have a disruption mitigation system that efficiently reduces the runaway generation.

The two experimentally most studied mitigation concepts are massive gas injection and pellet injection. The strategy in both these techniques is to inject a large amount of material in order to cool the plasma in a controlled way before a natural disruption would otherwise have taken place. Such controlled shut-down scenarios can significantly reduce the problems of non-uniform wall heat loads during the thermal quench phase and large vessel forces due to halo currents in the current quench phase [5–8]. In addition, the goal is that the injected material should raise the electron density to a high enough level to prevent runaway electron generation. However, before material injection can be used as a reliable means to suppress runaways in ITER-size tokamaks, there are several issues that need to be resolved. This concerns for instance how to achieve a suitable deposition profile of the appropriate materials inside the plasma. Moreover, the shear amount of material that needs to be introduced for complete runaway suppression poses a problem in ITER in particular because of vacuum pump limitations and extreme heat loads on the wall [9]. A further concern is that it is necessary to predict that a natural disruption is about to happen early enough, in order to initiate the controlled shut-down process before the disruption. This is indeed a non-trivial task [10], and it would be advantageous if the runaway suppression did not rely on this requirement.

In the present paper we investigate the possibility to use a passive technique to suppress runaways in disruptions. The idea, proposed in Ref. [11], is to construct the wall in such a way that any toroidal current it carries is forced to take a helical path. The large toroidal

electric field induced in a disruption then drives helical currents in the wall, creating magnetic islands in the plasma, which if they have sufficient overlap lead to ergodic regions and enhanced runaway losses. If the losses are large enough to balance the avalanche gain, large runaway currents can be avoided.

The helical wall structure would not affect the normal discharge because the toroidal electric field in the highly conducting pre-disruption plasma is very small (less than a tenth of a volt in ITER). The wall, with its lower conductivity, thus carries a very small current during the main discharge phase. In contrast, the loop voltage in the disruption is expected to be a hundred to a thousand volts, which gives a considerable wall current and large magnetic perturbations. One concern is that the plasma start-up phase could be negatively affected by helical wall currents, but it was noted in Ref. [11] that this will be a limited problem, because the ramp-up loop voltage is small (in ITER of order of a volt). In addition, the error field control coils could be used to compensate what little asymmetric field is driven by the start-up voltage.

The proposed technique would only address the runaway electron problem. To mitigate the heat load other methods would be required, e.g. gas or pellet injection. Large vessel forces could potentially also be an issue for the proposed passive method. However, the currents that are induced in the vessel during a disruption are large whether they are channelled in a roughly pitch-resonant path with the magnetic field or not. Channelling the currents into a roughly pitch-resonant path, as needed for magnetic surface break up, does not increase the forces on the vessel. Indeed, the forces would vanish if the currents were in exact pitch resonance. Moreover, since the vessel forces are related to the designed helical current paths in the wall, one can in principle calculate how the forces are distributed and construct the wall to withstand them.

A potential advantage with the proposed scheme could be that even if the other mitigation techniques fail, runaways will still be affected by the passive system, since the necessary electric field to drive the helical wall currents is inherently present in the disruption. The present study will show that it may not always be possible for the passive runaway suppression scheme to create island overlap regions in the central part of the plasma (where the runaways are created) in time to prevent a significant runaway current. However, the outer half of the plasma easily becomes ergodized, and the Ohmic current channel therefore contracts, which may lead to MHD instabilities that flush out the runaway electrons.

The passive runaway suppression strategy has similarities with the use of resonant magnetic perturbation (RMP) coils, in that both methods make use of currents outside the plasma to perturb the magnetic fields and inflict runaway losses. Both techniques also have to deal with the problem that magnetic islands form most easily at low order rational surfaces, which are initially very rare in the central part of the plasma, where runaway electrons tend to be created [12]. However, the helical currents driven by the disruption electric field in the passive scheme can be much larger than the currents used in RMP coils.

## II. MODEL

To assess the theoretical feasibility of the proposed scheme, we use a simple cylindrical model for the plasma and the surrounding conductors as shown in Fig. 1. The evolution of the current profile is followed using the code presented in [13], which calculates the evolution of the toroidal electric field $E$ and the runaway density when there is a prescribed sudden drop in conductivity $\sigma$ (e.g. a disruption). Inside the plasma, the induction equation

$$\frac{1}{r}\frac{\partial}{\partial r}\left(r\frac{\partial E}{\partial r}\right) = \mu_0 \frac{\partial j}{\partial t}, \tag{1}$$

is solved, where the current $j = \sigma E + n_{\mathrm{run}} ec$ consists of an Ohmic and a runaway electron part. The velocity space distribution of the runaway electrons is not modeled in detail. Only the total density of runaways $n_{\mathrm{run}}(r,t)$ is considered, and this density changes in time according to the well-known Dreicer [14] and avalanche generation rates [1]. In the present context, the calculation of the runaway density is only interesting in so far as it shows when the runaway current would have become a significant fraction of the original plasma current if no losses were to occur. Before this time, the aim is to create enough magnetic perturbations to cause the runaways to leave the plasma.

In the cylindrical model geometry in Fig. 1, the plasma radius is $r = a$ and the helically conducting wall is situated at $r = b$. Since $E$ varies linearly with $\ln r$ in vacuum in a cylindrical model, an ideally conducting wall is required at some outer radius $r = c$, which is taken to be of the order of the tokamak major radius. At $r = b$, a toroidal current is induced, for which the poloidally averaged surface current density $\bar{I}_{sb}$ is given by Eq. (1) as

$$\mu_0 \frac{d\bar{I}_{\mathrm{s}b}}{dt} = \left[\frac{\partial E}{\partial r}\right]_b, \tag{2}$$

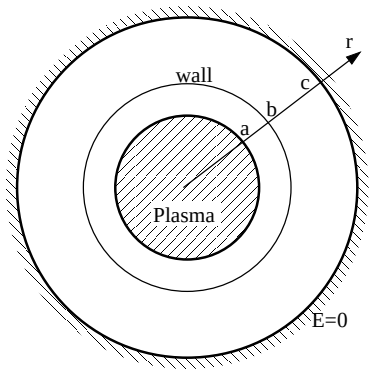


FIG. 1: Cylindrical model geometry

where the brackets denote a jump $[x]_b = x(r = b^+) - x(r = b^-)$. Equation (2) together with the vacuum variation of the electric field yield a relation between $E$, $\partial E/\partial r$ and $\partial E/\partial t$ at $r = a$. This relation is the boundary condition for the cylindrically symmetric part of the numerical calculation, which solves Eq. (1) inside the plasma using a Crank-Nicolson scheme to step forward in time on a radial grid.

### A. Helical wall currents

We want to create magnetic fields inside the plasma with several different poloidal and toroidal harmonics $m$ and $n$, and study whether the ensuing islands overlap. Not taking technological constraints into account, we of course have a lot of freedom in how to design the wall to achieve this, but we limit ourselves to simple geometries. A very simple helical wall structure, where the current follows straight lines in the $(\theta, \phi)$-plane would only give islands at one rational surface. In order to obtain perturbations at several $m$ and $n$, it is necessary to make the helix undulate or wiggle somewhat. In practice, such an irregular helical path would be unavoidable because of the many ports in the vessel. The current density at $r = b$ can be written as $\mathbf{j} = \delta(r - b)\nabla\kappa \times \nabla r$, where $\kappa(\theta, \phi)$ is the current potential. To create the necessary toroidal and poloidal "sidebands", we let the current potential be a function $\kappa(\xi)$, where $\xi$ is defined as

$$\xi \equiv N(\phi + \alpha \sin\phi) - M(\theta + \beta \sin\theta). \tag{3}$$

One can in general write $\kappa$ as

$$\kappa = \kappa_0 \xi + \sum_{p=1}^{\infty} i \frac{\kappa_p}{2} e^{-ip\xi} + \text{c.c.}, \tag{4}$$

where the $\kappa_0$ term is responsible for the net toroidal current. For simplicity, we only keep one term in the expansion, so that

$$\kappa = \kappa_0 \xi + \left( i \frac{\kappa_1}{2} e^{-i\xi} + \text{c.c.} \right) = \kappa_0 \xi + \kappa_1 \sin \xi. \tag{5}$$

Furthermore, to ensure that the toroidal current density

$$\begin{aligned} j_\phi &= -\delta(r-b) \frac{1}{b} \frac{\partial \kappa}{\partial \theta} = \\ &= \delta(r-b) \frac{M}{b} \left(1 + \beta \cos\theta\right) \left(\kappa_0 + \kappa_1 \cos\xi\right) \end{aligned} \tag{6}$$

is positive in our model we must have $|\beta| < 1$ and $\kappa_1 \leq \kappa_0$. We choose $\kappa_1 = \kappa_0$, so that there are separate current paths delineated by lines of zero current, which could correspond to slits or insulating bands made in the wall to guide the current. A Fourier decomposition of $\kappa$ in $\theta$ and $\phi$,

$$\kappa = \kappa_0 \xi + \left( \sum_{m,n} \kappa_{mn} e^{i(m\theta - n\phi)} + \text{c.c.} \right), \tag{7}$$

yields the coefficients

$$\begin{aligned} \kappa_{mn} &= \iint i \frac{\kappa_0}{2} e^{-i\xi} e^{-i(m\theta - n\phi)} \frac{d\theta d\phi}{4\pi^2} \\ &= \iint i \frac{\kappa_0}{2} e^{i[(n-N)\phi - N\alpha \sin\phi + (M-m)\theta + M\beta \sin\theta]} \frac{d\theta d\phi}{4\pi^2} \\ &= i \frac{\kappa_0}{2} J_{n-N}\left(N\alpha\right) J_{m-M}\left(M\beta\right). \end{aligned} \tag{8}$$

From Eq. (7) we now obtain the toroidal surface current density

$$I_{sb} = -\frac{1}{b} \frac{\partial \kappa}{\partial \theta} = \bar{I}_{sb} + \beta \bar{I}_{sb} \cos\theta + \sum_{m,n} I_{smn} \cos(m\theta - n\phi), \tag{9}$$

where the helically varying contributions to the surface current densities are

$$I_{smn} = \bar{I}_{sb} \frac{m}{M} J_{n-N}\left(N\alpha\right) J_{m-M}\left(M\beta\right), \tag{10}$$

and the net toroidal current in the shell is $I_b = 2\pi b \bar{I}_{sb} = 2\pi \kappa_0 M$. We neglect the effect of the term in Eq. (9) proportional to $\cos\theta$, because we consider a cylindrical model. In

reality, such an asymmetric current would shift the plasma towards the wall, and the closer proximity to the helical currents would then make it easier to break up the central magnetic surfaces than what follows from the present analysis. Figure 2 shows the current density for an example set of parameters $M = 3$, $N = 2$, $\alpha = 0.5$, $\beta = 0.9$, which is used as a reference case in the calculations. The values of $\alpha$ and $\beta$ were chosen to give a relatively large undulation to the $\xi$ =constant contours (see Fig. 2b), while keeping $d\theta/d\phi > 0$. In a more realistic situation, one would need to chose the current paths in the vessel so as to avoid too large forces on the structure. The force per wall area for the current potential (5) is

$$\begin{aligned} F &= B_{\rm tor}\frac{1}{R}\frac{\partial\kappa}{\partial\phi} - B_{\rm pol}\frac{1}{b}\frac{\partial\kappa}{\partial\theta} = \\ &= \frac{I_b B_{\rm tor}}{2\pi R}(1+\cos\xi)\left(\frac{N(1+\alpha\cos\phi)}{M} - \frac{1+\beta\cos\theta}{q(b)}\right), \end{aligned} \tag{11}$$

which can be as high as $\sim BI_b(1+\alpha)N/(\pi MR)$, but in the limit of small $\alpha$ and $\beta$ and $M/N \approx q(b)$ the force vanishes because the current is parallel to the magnetic field. There is a trade-off between producing islands at many rational surfaces, which requires large undulation of the current paths, and keeping the forces small, which requires small undulation. This may be alleviated in a more realistic geometry, where the plasma shaping helps to couple different poloidal mode number components of the perturbed magnetic field together [15], which reduces the need for current path undulation.

The currents are driven by the electric field $E$ calculated in Eq. (1). It is assumed that helical electric field components are much smaller than the symmetric component $E$, so that the $m, n$ perturbation does not cause any feedback to itself by inducing currents in the wall. The helical currents $I_{smn}$ are therefore directly proportional to $E$. The wall is modeled as a thin cylindrical shell with conductance $\sigma_{\rm wall}$ and thickness $d$. The thin shell approximation is valid when $d$ is smaller than the skin depth in the current quench (which for steel is $\sim 5-10$ cm in JET and $\sim 10-20$ cm in ITER). The symmetric part of the surface current density becomes $\bar{I}_{sb} = \sigma_{\rm wall} d\, E(b)$, and the $m, n$ component is therefore

$$I_{smn} = \sigma_{\rm wall} d\, E(b)\frac{m}{M} J_{n-N}\left(N\alpha\right) J_{m-M}\left(M\beta\right). \tag{12}$$

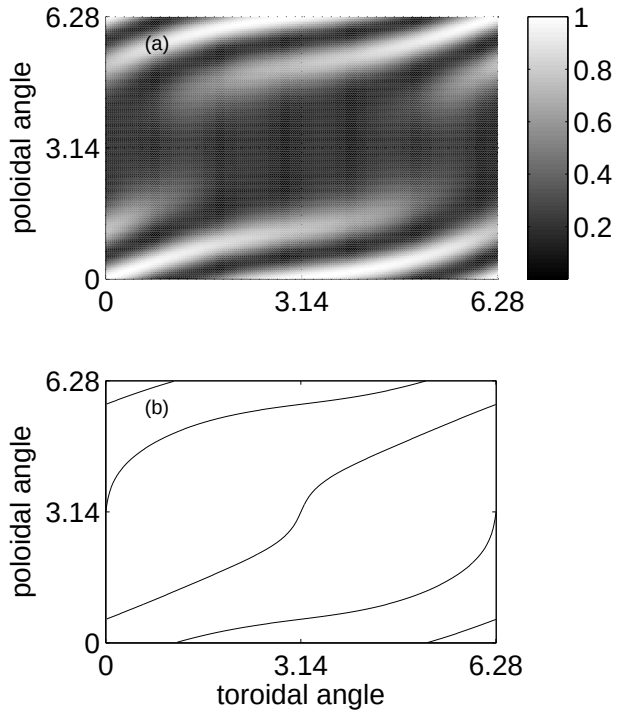


FIG. 2: a) Normalized surface current $j_\phi(\theta,\phi)$ for the example case $M = 3$, $N = 2$, $\alpha = 0.5$, $\beta = 0.9$. b) Corresponding zero current ($\xi = \pi$) contours.

### B. Magnetic field

The helical currents in the wall lead to helical fields in the plasma, which are here modeled using the magnetic vector potential (rather than the electric field as was done in Eq. (1) for the symmetric component). The toroidal component of the magnetic vector potential is expressed as

$$A = \sum_{m,n} A_{mn}(r,t)\cos(m\theta - n\phi). \tag{13}$$

In the plasma, the vector potential obeys the following differential equation

$$\frac{1}{r}\frac{\partial}{\partial r}r\frac{\partial}{\partial r}A_{mn} - \frac{m^2}{r^2}A_{mn} + \frac{R}{r}\frac{qm}{nq-m}\frac{dk_0}{dr}A_{mn} = 0, \tag{14}$$

where $k_0 = \mu_0 j/B$, see e.g. Ref. [16]. In the last term, which is singular at the rational surface radius $r_\mathrm{s}$ where $m = q(r_\mathrm{s})n$, we make the approximation

$$\frac{1}{n/m-\iota} \approx \frac{n/m-\iota}{(n/m-\iota)^2+\Delta_{mn}^2}, \tag{15}$$

where $\iota \equiv 1/q$ and $\Delta_{mn}$ is related to the island half-width $\delta_{mn}$ through $\Delta_{mn} = \delta_{mn} d\iota/dr|_{r_\mathrm{s}}$. The fact that the cold post-thermal quench plasma is highly resistive implies that the islands

have all reached their saturated half-widths [16]

$$\delta_{mn} = \sqrt{\frac{4R}{rB}\left|\frac{A_{mn}}{d\iota/dr}\right|}. \tag{16}$$

Since this half-width depends on the solution $A_{mn}$ to Eq. (14), the approximation (15) must be made iteratively.

In the vacuum regions, the singular term is absent in Eq. (14) and the solutions are $A_{mn} = Cr^{-m} + Dr^m$. The boundary condition $A_{mn} = 0$ at $r = c$ and the jump condition $\mu_0 I_{smn} = -[\partial A_{mn}/\partial r]_b$ at $r = b$ yield the following relation between $A_{mn}$ and $\partial A_{mn}/\partial r$ at the plasma edge

$$\begin{aligned} &-\mu_0 I_{smn} = \\ &\frac{m}{b} A_{mn}(a)\left(\coth m \ln\frac{b}{c}\cosh m\ln\frac{b}{a} - \sinh m\ln\frac{b}{a}\right) + \\ &+\frac{a}{b}\frac{\partial A_{mn}}{\partial r}(a)\left(\coth m\ln\frac{b}{c}\sinh m\ln\frac{b}{a} - \cosh m\ln\frac{b}{a}\right). \end{aligned} \tag{17}$$

The evolution of island sizes is determined by numerical solution of Eq. (14) inside the plasma with Eq. (17) as boundary condition. In the present simulations, radial transport of runaways due to the perturbed magnetic fields is not included, but as we will see, one can draw several important conclusions without including this effect. This is because the main difficulty is to generate the island overlap regions where the runaway electrons are. Once this hurdle has been overcome, one can begin to study how large the losses would be.

## III. RESULTS AND DISCUSSION

In a disruption simulation, we mimic the thermal quench phase of the disruption by prescribing the plasma temperature to fall exponentially to a small value $T_{\text{final}} = 10$ eV on a short time scale (1 ms in the case of JET). On this time scale, the resulting decrease in conductivity $\sigma$ cannot be compensated for by resistive diffusion, i.e., by the left-hand side of Eq. (1), so a high electric field is induced. On the longer, resistive time scale of the plasma $\sim a^2\mu_0\sigma$, the electric field diffuses according to Eq. (1), and the Ohmic plasma current quenches. The resistive time of the wall is even longer ($\sim \mu_0\sigma_{\text{wall}} d\, b \ln(c/b)$), so initially, the part of the lost Ohmic plasma current which is not replaced by runaway current will be driven as the current $I_b$ in the wall. On the resistive time scale of the wall, the wall current $I_b$ is eventually replaced by a current $I_c$ in the outer conductor at $r = c$.

These current dynamics can be studied in Fig. 3a for a simulation with the JET-like parameters $I_0 = 1.9$ MA, $B = 3.5$ T, $n_\mathrm{e} = 3 \cdot 10^{19}$ m$^{-3}$, $T_\mathrm{final} = 10$ eV, $d = 5$ cm, $R = 3$ m, $a = 1$ m, $b = 1.3$ m and $c = 3$ m. Figure 3a shows that without losses, the runaway current becomes significant at around 6 ms, so ideally the desired runaway loss mechanism should become active before that. Otherwise, the peaked runaway current profile in Fig. 3b will result.

The helical current density components $I_{smn}$ in the wall are proportional to $I_b$, and the solution of Eqs. (14–17) with $I_{smn}$ in the boundary condition (17) results in the islands indicated in Fig. 3c. In the first millisecond we do not display any islands, because the plasma is still hot and the island saturation time is not short compared to the other time scales, invalidating the use of Eq. (16). Moreover, it is likely that the thermal quench is caused by large internal islands, which should then, in principle, be included in the simulation. These pre-existing islands could make it easier for the externally generated non-axisymmetric fields to ergodize the plasma. However, after the temperature drop, the initial islands can be expected to quickly decay away on the Rutherford time scale, so we do not consider them here.

One sees that, in the Fig. 3 example, island overlap regions start to form at around the time when the runaway beam current appears, but only in the outer half of the plasma because of the higher density of rational surfaces there. Later, when the runaway current is larger, a $q = 1$ surface appears, and a more centrally situated island forms. The Poincaré plots in Figs. 3d and e at the times $t = 5.3$ ms when $I_\mathrm{run}/I_0 = 1\%$ and at 6.8 ms when $I_\mathrm{run}/I_0 = 15\%$ of the initial current, respectively, also indicate that the central region, where the runaway electrons appear, does not become ergodic. This example is therefore discouraging for the use of this type of passive mitigation scheme.

However, the simulation result is sensitive to input parameters such as, for instance, the electron density. It is interesting to vary this parameter in particular, since injection of gas or pellets (which may be necessary for mitigation of heat or mechanical loads) would increase the electron density. The slightly higher density $n_\mathrm{e} = 5 \cdot 10^{19}$ m$^{-3}$ chosen in Fig. 4, yields a higher ergodicity in the inner plasma when the runaway current has reached appreciable levels (an increased $T_\mathrm{final}$ gives similar results). The reason is not only that the higher density results in a lower runaway current, but also that it appears at a later time when the wall current has increased and created ergodic regions, see Fig. 4a. Perhaps even

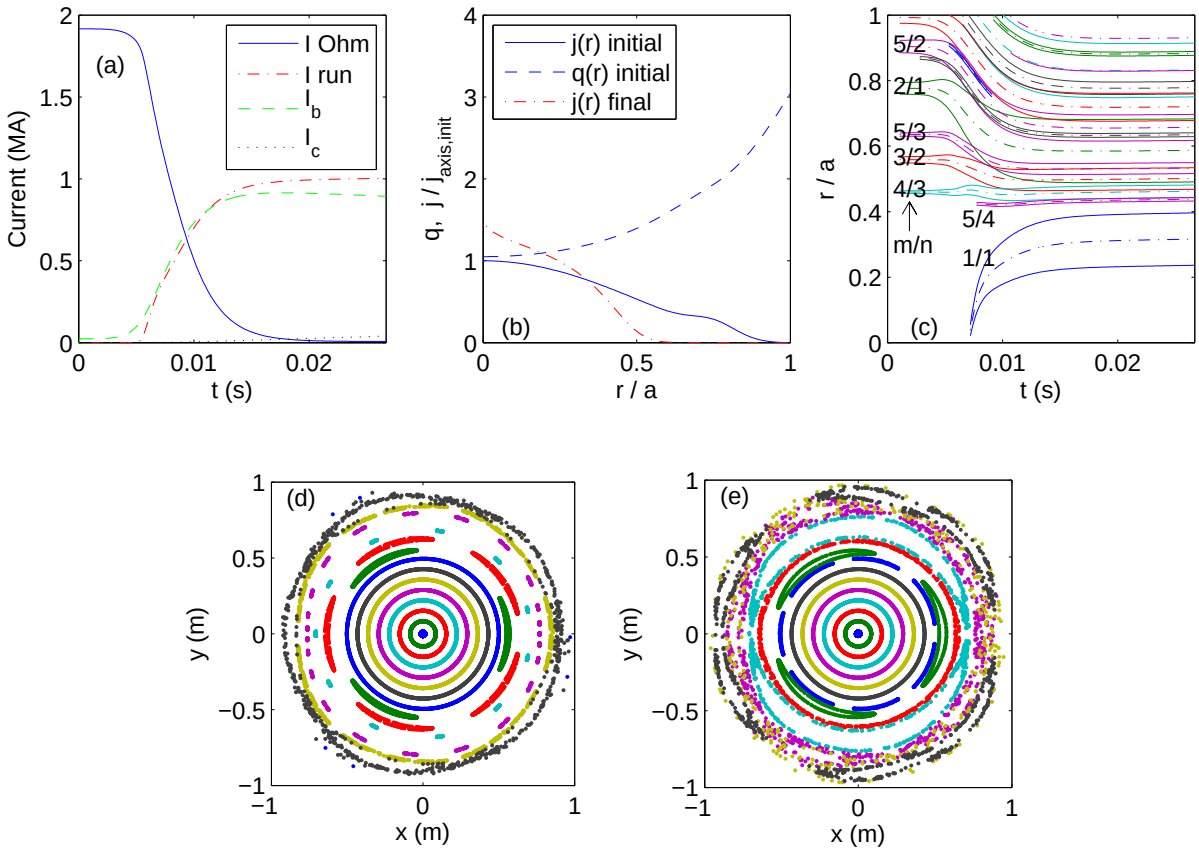


FIG. 3: a) Evolution of Ohmic current, runaway current and wall currents at $r = b$ and $r = c$. b) Initial current density profile (red), q profile (red dashed) and post-CQ runaway current profile (black). The little bump was added to the initial current profile to avoid an unstable $m = 2, n = 1$ mode. c) Rational surface positions (dash-dotted) and corresponding islands (solid). Only islands with $\delta_{mn}/a > 5 \cdot 10^{-3}$ are shown. Colors (online) represent $m = 1, 2, 3 \ldots$ as blue, green, red, cyan, magenta, yellow, black.... d) and e) Poincaré plots at the times when $I_{\mathrm{run}}/I_0 = 1\%$ and 15% respectively. Different colors (online) represent different field lines.

more importantly, the lower primary generation leads to a more peaked radial profile of the runaway current [13] and the rational surfaces therefore move closer to the center. However, the potential increase in runaway losses this could lead to is counteracted to some extent by the fact that the runaways are also more centrally located.

The outcome also depends on the helical structure of the wall. Figures 5a and b show the islands for the same case as in Fig. 3 but with $M = 2$, $N = 1$ and $M = 1$, $N = 1$, respectively. In general, lower $M$ and $N$ tend to yield fewer but larger islands. At times

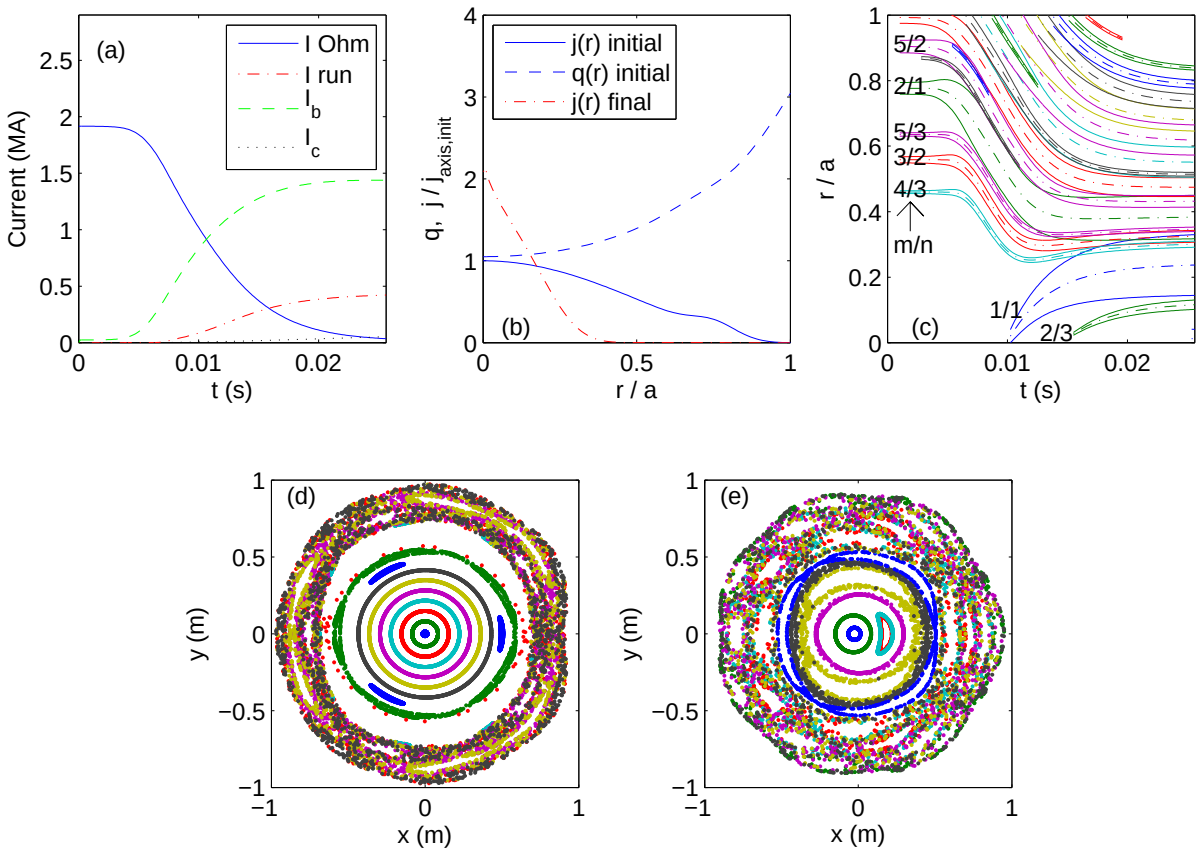


FIG. 4: The same as Fig. 3 but with $n_e = 5 \cdot 10^{19}$ m$^{-3}$.

when the peaked runaway current has already formed and resulted in the appearance of a $q = 1$ surface, one sees that the $M = 1$, $N = 1$ option creates the largest island overlap region. However, before the runaway current becomes significant, only the outer half of the plasma becomes ergodic, regardless of $M$ and $N$. (We note that the stability properties and the calculated island size at $q = 1$ are not very accurate in a cylindrical model.)

The parameters $\alpha$ and $\beta$ in our simple wall current model are responsible for creating islands at sufficiently many rational surfaces. If these parameters are chosen too small, mostly the the $q = M/N$ surface is affected. Another geometric property that can affect the size of the chaotic regions is plasma elongation. This effect is not studied in the present paper, but it has been seen in other works that elongation tends to enhance runaway losses [17].

One effect that can give early runaway losses is if the changes in the current profile leads to MHD instability. If the current in the outer half of the plasma is lost because of the ergodic magnetic field, then the current channel shrinks considerably. This contraction may

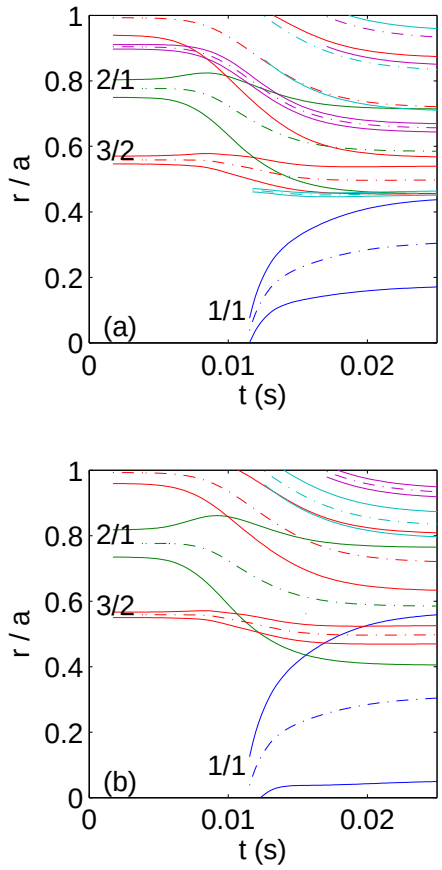


FIG. 5: Islands for the case in Fig. 3 with a) $M = 2$, $N = 1$ and b) $M = 1$, $N = 1$

happen already before the runaways have started to contribute to the current. To study if this results in instability without going into details on how the islands affect the current profile, we do the following. In the simulation presented in Fig. 3, a line $r_c(t)$ is manually drawn, outside which the magnetic field is assessed to be ergodic enough. In this outer region, the resistivity is increased by a large factor, so that the current density becomes reduced to a very low level. The outer part $r > r_c$ is now regarded as belonging to the vacuum region, and when a rational surface crosses the boundary into the vacuum, the corresponding $m/n$ mode may become unstable to an external kink mode.

The line $r_c(t)$ is shown in black in Fig. 6a and the final current density profile in Fig. 6b indicates that the current has been removed from $r > r_c$. Stability is determined by the criterion that $A_{mn}(r_c)[dA_{mn}/dr]_{r_c} < 0$ when the solution for inner radii is patched to a decaying $r^{-m}$ solution for $r > r_c$. For the rational surfaces where an external kink mode is unstable when $r_s > r_c$, the dash-dotted line in Fig. 6a, which shows the position of the

rational surface, has been continued as long as the simulated current profile yields instability. We observe for instance that the green dash-dotted line indicates that the $m = 2$, $n = 1$ mode becomes unstable at $t = 9$ ms. At that time we thus expect the occurrence of large scale MHD activity that will destroy the nested flux surfaces and reduce the number of runaways drastically. However, it is not known how much of the runaway beam is lost, or if nested flux surfaces will form again after this event.

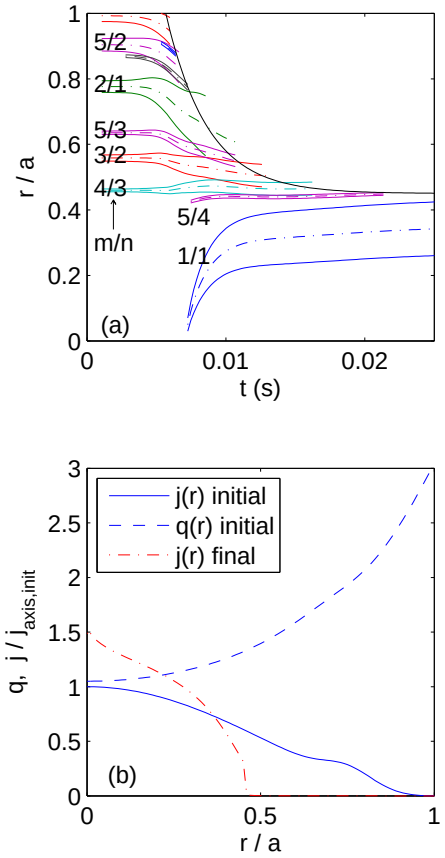


FIG. 6: a) The plasma current has been removed in the outer region $r > r_c(t)$ delineated by the black line. The lines showing rational surface positions (dash-dotted) have been drawn in the region $r > r_c(t)$ only where the corresponding external kink mode is unstable. An $m = 2$, $n = 1$ mode (green) is seen to become unstable at $t \simeq 9$ ms, which means that the simulation after this time is of limited relevance. b) Current density and q profiles. Note that the final current profile is practically zero in the outer half as intended.

Finally, Fig. 7 presents a simulation for an ITER-like plasma with $I_0 = 15$ MA, $B = 5.3$ T, $n_e = 8 \cdot 10^{19}$ m$^{-3}$, $T_{final} = 10$ eV, $d = 10$ cm, $R = 6.2$ m, $a = 2.7$ m, $b = 3.1$ m, $c = 5$ m.

This is a simulation which, like the one in Fig. 4, has a rather modest primary runaway generation and therefore a highly peaked final runaway current density profile, see Fig. 7b. Figures 7a and c show that the rational surfaces move inward already before the runaway current becomes significant, but because of the $r^m$ dependence of $A_{mn}$ at small $r$, the islands shrink as they approach the center. The major island overlap regions therefore remain in the outer half of the plasma until the time when the runaway current starts to influence the q-profile. The Poincaré plot in Fig. 7d shows that when the runaway current is around 7% of the initial current, also the central part is ergodic. (Remember that the runaway transport due to the ergodic field is not included here.) Moreover, also in this ITER-like case, the results depend on the parameters and the physics included in the model. If other primary sources, such as e.g. hot-tail runaway generation are important, one expects a less peaked profile [18] and ergodic regions that are situated at larger radii.

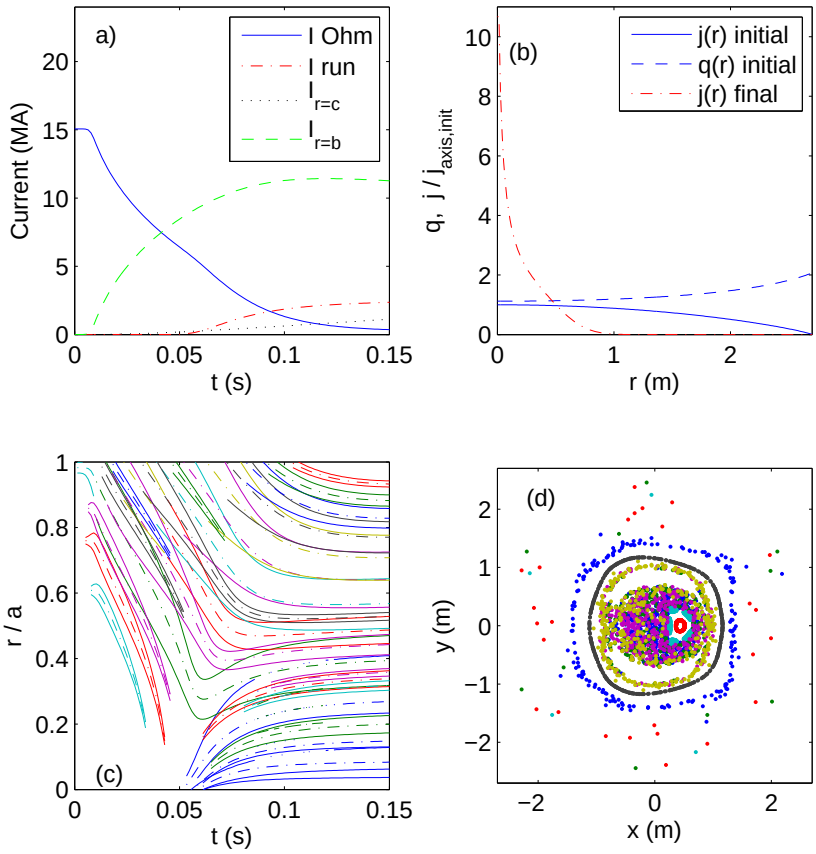


FIG. 7: ITER simulation. Plots a), b) and c) are of the same kind as in Fig. 3. d) Poincaré plot at 75 ms, when $I_{\rm run}/I_0 \simeq 7\%$.

## IV. CONCLUSIONS

The helical wall currents make the outer half of the plasma cross section ergodic under many circumstances. However, to create large island overlap regions in the central plasma where the runaway beam forms is difficult, because the density of low order rational surfaces is initially very low in the center. To make the few centrally located rational surfaces display large islands one needs to make the main periodicity numbers of the wall, $M$ and $N$, small. The success in ergodizing the more central regions before the time when runaway electron current becomes significant also depends on parameters such as electron density and post-thermal quench temperature. Parameters that lead to less efficient primary runaway generation tend to yield more peaked runaway current profiles and thus ergodic regions closer to the axis.

A combination of the presented scheme with other disruption mitigation schemes would thus be advantageous. In order for such a combination to be considered passive, one would need to devise a material injection scheme that is triggered by the disruption. We have seen that the electron density increase required for the helical currents to significantly ergodize the magnetic field is of the order of the pre-exiting plasma density, as opposed to a hundred times more, which would be needed to guarantee $E < E_{\mathrm{c}}$ in ITER [10]. The material injection device could therefore possibly be a simpler contraption than the existing systems. It could for instance be a wall component that gives off a suitable material in a disruption, acting as a "fuse", i.e., an element that can be sacrificed and replaced.

The proposed passive technique may be successful in its own right in another way. We have seen that it is likely that the contraction of the Ohmic current profile before the major runaway current formation results in MHD instabilities. These instabilities would flush out a large part of the existing runaway population. Finally, we note that the results presented here may underestimate the efficiency of the passive scheme, since plasma shaping [17] and the associated coupling between different poloidal mode number components [15] are not taken into account. Further investigations to more accurately assess the feasibility of the passive technique would need to include this mode coupling.

**Acknowledgements**

This work was carried out under the auspices of the Max-Planck/Princeton Center for Plasma Physics.

---

[1] M. N. Rosenbluth and S. V. Putvinski, Nucl. Fusion **37**, 1355 (1997).

[2] P. Helander, L.-G. Eriksson, and F. Andersson, Plasma Phys. Control. Fusion **44**, B247 (2002).

[3] L.-G. Eriksson, P. Helander, F. Andersson, D. Anderson, and M. Lisak, Phys. Rev. Lett. **92**, 205004 (2004).

[4] J. Riemann, H. M. Smith, and P. Helander, Phys. Plasmas **19**, 012507 (2012).

[5] E. M. Hollmann, T. C. Jernigan, M. Groth *et al.*, Nucl. Fusion **45**, 1046 (2005).

[6] D. G. Whyte, R. Granetz, M. Bakhtiari, V. Izzo, T. Jernigan, J. Terry, M. Reinke, and B. Lipschultz, J. Nucl. Mater. **363-365**, 1160 (2007).

[7] R. Granetz, E. Hollmann, D. Whyte *et al.*, Nucl. Fusion 1086 (2007).

[8] G. Pautasso, D. Coster, T. Eich *et al.*, Plasma Phys. Control. Fusion **51**, 124056 (2009).

[9] S. Putvinski, L. Baylor, D. Campbell *et al.*, in *Proc. of the 23th IAEA Fusion Energy Conference 2010, Daejon* (IAEA, Vienna, 2010), pp. IAEA–CN–180/ITR/1–6.

[10] T. C. Hender, J. C. Wesley, J. Bialek *et al.*, Nucl. Fusion **47**, S128 (2007).

[11] A. H. Boozer, Plasma Phys. Control. Fusion **53**, 084002 (2011).

[12] G. Papp, M. Drevlak, T. Fülöp, and G. I. Pokol, Plasma Phys. Control. Fusion **54**, 125008 (2012).

[13] H. Smith, P. Helander, L.-G. Eriksson, D. Anderson, M. Lisak, and F. Andersson, Phys. Plasmas **13**, 102502 (2006).

[14] J. W. Connor and R. J. Hastie, Nucl. Fusion **15**, 415 (1975).

[15] J.-K. Park, A. H. Boozer, J. E. Menard, and M. J. Schaffer, Nucl. Fusion **48**, 045006 (2008).

[16] A. H. Boozer, Rev. Mod. Phys. **64**, 1071 (2004).

[17] V. Izzo, E. Hollmann, A. James *et al.*, Nucl. Fusion **51**, 063032 (2011).

[18] H. Smith and E. Verwichte, Phys. Plasmas **15**, 072502 (2008).